Supplemental Document: Frame-Free Directional Mueller Calculus using Polarized Spherical Harmonics

SHINYOUNG YI, KAIST, South Korea and Kyung Hee University, South Korea
JIWOONG NA, KAIST, South Korea
SEUNGMIN HWANG, KAIST, South Korea
INSEUNG HWANG, KAIST, South Korea
MIN H. KIM, KAIST, South Korea

ACM Reference Format:
Shinyoung Yi, Jiwoong Na, Seungmin Hwang, Inseung Hwang, and Min H. Kim. 2025. Supplemental Document: Frame-Free Directional Mueller Calculus using Polarized Spherical Harmonics. *ACM Trans. Graph.* 44, 6, Article 177 (December 2025), 10 pages. https://doi.org/10.1145/3763276

A FORMULAE FOR FRAME FIELDS

Frame fields are functions that describe local frames along the ray directions. The definition of frame fields is $\vec{\mathbf{F}} \in \hat{\mathbb{S}}^2 \to SO(3)$, where $\vec{\mathbf{F}}(\hat{\omega})\hat{z}_g = \hat{\omega}$ which means Frame field output should be the rotation which transforms z axis to ray direction. The first and second angles of ZYZ Euler angles determine the transform of the z-axis, and the last angle gives a degree of freedom of the local frames. Therefore, the frame fields can be described as the function from ray direction to the last angle of ZYZ Euler angles. The exact formulae of typical frame fields are as follows:

$$\vec{\mathbf{F}}_{\theta\phi}(\theta,\phi) = \vec{\mathbf{F}}_g \mathbf{R}_{zyz}(\phi,\theta,0), \tag{1a}$$

$$\vec{\mathbf{F}}_{\phi\theta}(\theta,\phi) = \vec{\mathbf{F}}_g \mathbf{R}_{zyz}\left(\phi,\theta,\frac{\pi}{2}\right), \tag{1b}$$

$$\vec{\mathbf{F}}_{\text{geo}}(\theta,\phi) = \vec{\mathbf{F}}_g \mathbf{R}_{zyz}(\phi,\theta,-\phi), \text{ and} \tag{1c}$$

$$\vec{\mathbf{F}}_{\text{Duff}}(\theta,\phi) = \begin{cases} \vec{\mathbf{F}}_g \mathbf{R}_{zyz}(\phi,\theta,-\phi) & \theta \le \frac{\pi}{2} \\ \vec{\mathbf{F}}_g \mathbf{R}_{zyz}(\phi,\theta,\phi-\pi) & \theta > \frac{\pi}{2} \end{cases}. \tag{1d}$$

B EXACT FORMULAE FOR S2L2 REPRESENTATION

Here we provide exact formulae to compute Equations (13) and (14) in the main paper for the sake of reproducibility and completeness.

It will be helpful for readers about to reproduce our S2L2 representation method without any background of (spin-weighted) spherical harmonics (SH).

Authors' Contact Information: Shinyoung Yi, KAIST, South Korea and Kyung Hee University, South Korea, syyi@khu.ac.kr; Jiwoong Na, KAIST, South Korea, jwna@vclab.kaist.ac.kr; Seungmin Hwang, KAIST, South Korea, smhwang@vclab.kaist.ac.kr; Inseung Hwang, KAIST, South Korea, ishwang@vclab.kaist.ac.kr; Min H. Kim, KAIST, South Korea, minhkim@vclab.kaist.ac.kr.

ACM 1557-7368/2025/12-ART177
https://doi.org/10.1145/3763276

B.1 Spin-2 SH with Order $l = 2$

Before introducing formulae for spin-2 SH, we should discuss how to numerically describe values of a Stokes vector field at each point (direction). Only considering s_1 and s_2 components (spin-2 Stokes vectors rather than the full ones) for simplicity, there can be three ways to understand a Stokes vector field:

(1) *Physical, but abstract*: $\overleftrightarrow{f} : \hat{\mathbb{S}}^2 \to \mathcal{S}$, where $\mathcal{S}$ denotes the formally defined *Stokes space* [Mojzík et al. 2016; Yi et al. 2024] using equivalence classes.
(2) *Function of rotations*: $[f_1, f_2]^T : SO(3) \to \mathbb{R}^2$ with a constraint that:

$$\begin{bmatrix} f_1(\mathbf{R}\mathbf{R}_z(\psi)) \\ f_2(\mathbf{R}\mathbf{R}_z(\psi)) \end{bmatrix} = \begin{bmatrix} \cos 2\psi & \sin 2\psi \\ -\sin 2\psi & \cos 2\psi \end{bmatrix} \begin{bmatrix} f_1(\mathbf{R}) \\ f_2(\mathbf{R}) \end{bmatrix}, \quad \text{where } \mathbf{R}_z(\psi) \coloneqq \begin{bmatrix} \cos\psi & -\sin\psi & 0 \\ \sin\psi & \cos\psi & 0 \\ 0 & 0 & 1 \end{bmatrix}. \tag{2}$$

Here, a rotation matrix $\mathbf{R} \in SO(3)$ indicates a local frame $\vec{\mathbf{F}}_g\mathbf{R}$ at a point $\hat{z}_g$.
(3) *Fix a frame field*, then $[f_1, f_2]^T : \hat{\mathbb{S}}^2 \to \mathbb{R}^2$ can describe a Stokes vector field.

While the first way is more suitable to understand Stokes vector fields as geometric (physical) objects, other ones are more close to what data is actually stored in our implementation.

B.1.1 Formula under $\theta\phi$-frame field. Following Equation (3) proposes the third way to describe spin-2 SH basis functions with respect to a fixed $\theta\phi$-frame field.

$${}_2Y_{2,-2}(\theta,\phi) = \frac{1}{8}\sqrt{\frac{5}{\pi}}\left(1+2\cos\theta+\cos^2\theta\right)e^{-2i\phi} \tag{3a}$$

$${}_2Y_{2,-1}(\theta,\phi) = \frac{1}{4}\sqrt{\frac{5}{\pi}}\sin\theta\left(-1-\cos\theta\right)e^{-i\phi} \tag{3b}$$

$${}_2Y_{20}(\theta,\phi) = \frac{1}{4}\sqrt{\frac{15}{2\pi}}\sin^2\theta \tag{3c}$$

$${}_2Y_{21}(\theta,\phi) = \frac{1}{4}\sqrt{\frac{5}{\pi}}\sin\theta\left(-1+\cos\theta\right)e^{i\phi} \tag{3d}$$

$${}_2Y_{22}(\theta,\phi) = \frac{1}{8}\sqrt{\frac{5}{\pi}}\left(1-2\cos\theta+\cos^2\theta\right)e^{+2i\phi} \tag{3e}$$

where ${}_2Y_{lm} \coloneqq \left[\overleftrightarrow{Y}_{lm}\right]^{\vec{\mathbf{F}}_{\theta\phi}}$.

B.1.2 As a Function of Rotations. In many cases, we already has our measurement frame (local frames) $\vec{\mathbf{F}} \in \vec{\mathbb{F}}^3$ and then want Stokes parameters with respect to such frame $\vec{\mathbf{F}}$. Here we introduce two ways.

Computation using Euler angles. The first way is utilizing ${}_2Y_{lm}(\theta,\phi)$, which indicates complex-values Stokes parameters $s_1 + is_2$ with respect to the $\theta\phi$-frame field $\vec{\mathbf{F}}_{\theta\phi}$. Then we can convert it with respect to the frame $\vec{\mathbf{F}}$ using the angle between these two frames, i.e.,

$$ {}_2Y_{lm}\left(\vec{\mathbf{F}}\right) \coloneqq \left[\overset{\leftrightarrow}{Y}_{lm}\left(\vec{\mathbf{F}}\hat{z}_g\right)\right]^{\vec{\mathbf{F}}} = {}_2Y_{lm}(\theta,\phi)\, e^{-2i\psi}, \tag{4} $$

$$ \text{where } \vec{\mathbf{F}} = \vec{\mathbf{F}}_{\theta\phi}\begin{bmatrix}\cos\psi & -\sin\psi & 0\\ \sin\psi & \cos\psi & 0\\ 0 & 0 & 1\end{bmatrix}. \tag{5} $$

Note that $\vec{\mathbf{F}}_g = \begin{bmatrix}\hat{x}_g & \hat{y}_g & \hat{z}_g\end{bmatrix}$ denotes the global (world) frame, so that $\vec{\mathbf{F}}\hat{z}_g$ indicates the ray direction (local z-axis) of the measurement frame $\vec{\mathbf{F}}$ and θ, ϕ, and ψ can be obtained from ZYZ Euler angles of the rotation $\vec{\mathbf{F}}$ with respect to $\vec{\mathbf{F}}_g$, i.e.,

$$ \vec{\mathbf{F}} = \vec{R}_{\hat{z}_g\hat{y}_g\hat{z}_g}(\phi,\theta,\psi)\,\vec{\mathbf{F}}_g. \tag{6} $$

Since $\vec{\mathbf{F}}_g$ is the world frame, we can simply consider it a the 3D identity matrix in the numerical implementation.

Note that spin-2 SH under other frame fields can be also easily computed using Equation (1).

Computation using quaternions. However, there is more elegant implementation using quaternion representation $\mathbf{q} = q_0 + q_1 i + q_2 j + q_3 k$ of the rotation $\vec{R}$ such that $\vec{\mathbf{F}} = \vec{R}\vec{\mathbf{F}}_g$. Simply denoting ${}_2Y_{lm}(\mathbf{q}) = {}_2Y_{lm}\left(\vec{\mathbf{F}}\right)$, the following formula can be driven through some detailed steps. Using two auxiliary complex numbers $\mathbf{q}_a = q_0 + q_3 i$ and $\mathbf{q}_b = q_2 + q_1 i$, spin-2 SH can be evaluated as follows [Boyle 2013]:

$$ {}_2Y_{2,-2}(\mathbf{q}) = \sqrt{\frac{5}{4\pi}}\bar{\mathbf{q}}_a^4 \tag{7a} $$

$$ {}_2Y_{2,-1}(\mathbf{q}) = -\sqrt{\frac{5}{\pi}}\bar{\mathbf{q}}_a^3\bar{\mathbf{q}}_b \tag{7b} $$

$$ {}_2Y_{20}(\mathbf{q}) = \sqrt{\frac{15}{2\pi}}\bar{\mathbf{q}}_a^2\bar{\mathbf{q}}_b^2 \tag{7c} $$

$$ {}_2Y_{21}(\mathbf{q}) = -\sqrt{\frac{5}{\pi}}\bar{\mathbf{q}}_a\bar{\mathbf{q}}_b^3 \tag{7d} $$

$$ {}_2Y_{22}(\mathbf{q}) = \sqrt{\frac{5}{4\pi}}\bar{\mathbf{q}}_b^4 \tag{7e} $$

B.2 S2L2 Representation to Stokes Parameters

Given Stokes vector $\overset{\leftrightarrow}{s} = [\mathbf{s}]_{\vec{\mathbf{F}}}$, its 12-parameter S2L2 representation $\mathbf{r} = \text{S2L2}^C\left(\overset{\leftrightarrow}{s}\right) \in \mathbb{R}^{12}$ is characterized as:

$$ r_0 = s_0, \tag{8a} $$

$$ \begin{bmatrix}r_1\\ r_2\end{bmatrix} = \sqrt{\frac{4\pi}{5}}\mathbb{R}^2\left({}_2Y^C_{2,-2}\left(\vec{\mathbf{F}}\right)^*(s_1+is_2)\right), \tag{8b} $$

$$ \begin{bmatrix}r_3\\ r_4\end{bmatrix} = \sqrt{\frac{4\pi}{5}}\mathbb{R}^2\left({}_2Y^C_{2,-1}\left(\vec{\mathbf{F}}\right)^*(s_1+is_2)\right), \tag{8c} $$

$$ \begin{bmatrix}r_5\\ r_6\end{bmatrix} = \sqrt{\frac{4\pi}{5}}\mathbb{R}^2\left({}_2Y^C_{20}\left(\vec{\mathbf{F}}\right)^*(s_1+is_2)\right), \tag{8d} $$

$$ \begin{bmatrix}r_7\\ r_8\end{bmatrix} = \sqrt{\frac{4\pi}{5}}\mathbb{R}^2\left({}_2Y^C_{21}\left(\vec{\mathbf{F}}\right)^*(s_1+is_2)\right), \tag{8e} $$

$$ \begin{bmatrix}r_9\\ r_{10}\end{bmatrix} = \sqrt{\frac{4\pi}{5}}\mathbb{R}^2\left({}_2Y^C_{22}\left(\vec{\mathbf{F}}\right)^*(s_1+is_2)\right), \text{ and} \tag{8f} $$

$$ r_{11} = s_3, \tag{8g} $$

where $\mathbb{R}^2$ denotes conversion from complex numbers to 2D numeric real vectors as $\mathbb{R}^2(x+yi) = [x,y]^T$.

B.3 Stokes Parameters to S2L2 Representation

Given S2L2 representation $\mathbf{r}$ and objective local frame $\vec{\mathbf{F}}$, its projection to Stokes vector $\mathbf{s} = \text{S2L2Inv}^C\left(\mathbf{r};\vec{\mathbf{F}}\right) \in \mathbb{R}^4$ is represented as:

$$ s_0 = r_0, \tag{9a} $$

$$ \begin{bmatrix}s_1\\ s_2\end{bmatrix} = \sqrt{\frac{4\pi}{5}}\mathbb{R}^2\left(\sum_{m=-2}^{2}{}_2Y^C_{2m}\left(\vec{\mathbf{F}}\right)(r_{2m+5}+ir_{2m+6})\right), \text{ and} \tag{9b} $$

$$ s_3 = r_{11}. \tag{9c} $$

C PROOF OF PROPERTIES OF S2L2 REPRESENTATION

Left invertibility.

Proof: Recall:

$$ \text{S2L2Inv}^C(\mathbf{r};\hat{\omega}) = r_0 \oplus \underbrace{\left(\sqrt{\frac{4\pi}{5}}\sum_{m=-2}^{2}\sum_{p=1}^{2} r_{2m+p+4}\overset{\leftrightarrow}{Y}_{2mp}\right)}_{=:\text{S2L2Inv}_{1:2}} \oplus r_{11}. $$

(14 in the main paper, revised)

We only have to show $\text{S2L2Inv}_{1:2} = \overset{\leftrightarrow}{s}_{1:2}$. Using formulae under the $\theta\phi$-frame field (Equation (3)),

$$ \text{S2L2Inv}_{1:2} = \sqrt{\frac{4\pi}{5}}\mathbb{R}^2\left(\sum_{m=-2}^{2}{}_2Y_{2m}(\theta,\phi)\,(r_{2m+5}+ir_{2m+6})\right). \tag{10} $$

Here, $r_{2m+5+ir_{2m+6}}$ i.e., $r_1 + ir_2$, ..., $r_9 + ir_{10}$ can be rewritten as follows using Equation (8):

$$r_{2m+5} + ir_{2m+6} = \sqrt{\frac{4\pi}{5}}\,{}_2Y_{2m}(\theta,\phi)^*\,(s_1 + is_2)\,. \tag{11}$$

Then:

$$\begin{aligned}\mathrm{S2L2Inv}_{1:2} &= \sqrt{\frac{4\pi}{5}}\mathbb{R}^2\left(\sum_{m=-2}^{2} {}_2Y_{2m}(\theta,\phi)\sqrt{\frac{4\pi}{5}}\,{}_2Y_{2m}(\theta,\phi)^*\,(s_1+is_2)\right)\\ &= \frac{4\pi}{5}\sum_{m=-2}^{2}\left|{}_2Y_{2m}(\theta,\phi)\right|^2\begin{bmatrix}s_1\\ s_2\end{bmatrix}\end{aligned}. \tag{12}$$

The remaining part can be shown straightforwardly using Equation (3).

$$\left|{}_2Y_{2,-2}\right|^2 + \left|{}_2Y_{22}\right|^2 = \frac{5}{32\pi}\left[\left(1+\cos^2\theta\right)^2 + 4\cos^2\theta\right] \tag{13}$$

$$\left|{}_2Y_{2,-1}\right|^2 + \left|{}_2Y_{21}\right|^2 = \frac{5}{8\pi}\sin^2\left(1+\cos^2\theta\right) \tag{14}$$

$$\left|{}_2Y_{20}\right|^2 = \frac{15}{32\pi}\sin^4\theta \tag{15}$$

Gathering the common factor,

$$\begin{aligned}&\sum_{m=-2}^{2}\left|{}_2Y_{2m}(\theta,\phi)\right|^2 / \frac{5}{32\pi}\\ &= \underbrace{\left(1+\cos^2\theta\right)^2}_{1+2\cos^2\theta+\cos^4\theta} + \underbrace{4\cos^2\theta + 4\sin^2\theta}_{\text{Use }\cos^2\theta+\sin^2\theta=1}\left(1+\cos^2\theta\right) + 3\sin^4\theta\\ &= 5 + \underbrace{\cos^4\theta}_{\cos^2\theta(1-\sin^2\theta)} + 2\cos^2\theta + 4\sin^2\theta\cos^2\theta + \underbrace{3\sin^4\theta}_{3\sin^2\theta(1-\cos^2\theta)}\\ &= 5 + 3\cos^2\theta + 3\sin^2\theta = 8.\end{aligned} \tag{16}$$

Thus,

$$\sum_{m=-2}^{2}\left|{}_2Y_{2m}(\theta,\phi)\right|^2 = \frac{5}{4\pi}, \tag{17}$$

$$\mathrm{S2L2Inv}_{1:2} = \begin{bmatrix}s_1\\ s_2\end{bmatrix}. \tag{18}$$

□

Norm preservation.

Proof:

$$\begin{aligned}\sum_{i=1}^{10} r_i^2 &= \left\|\mathrm{S2L2}_{1:2}\left(\overleftrightarrow{s}\right)\right\|^2\\ &\underset{\text{Eq. (8)}}{\uparrow} = \frac{4\pi}{5}\sum_{m=-2}^{2}\left|{}_2Y_{2m}(\theta,\phi)\right|^2\left(s_1^2+s_2^2\right)\\ &\underset{\text{Eq. (17)}}{\uparrow} = s_1^2 + s_2^2\end{aligned} \tag{19}$$

□

Fiberwise linearity. $\mathbb{R}$-Linearity properties are straightforward. It comes from the property of the basis functions.

Note that $\mathbb{C}$-linearity, which was briefly described as a plan text in the main paper, can be concretely stated as follows. Note that for a spin-2 Stokes vector $\overleftrightarrow{s}_{1:2} = [\mathbf{s}_{1:2}]_{\vec{\mathbf{F}}}$, the following complex multiplication is well defined independent of choices of the local frame $\vec{\mathbf{F}}$:

$$z\overleftrightarrow{s}_{1:2} \coloneqq \left[\mathbb{R}^{2\times2}(z)\,\mathbf{s}_{1:2}\right]_{\vec{\mathbf{F}}} = \left[\mathbb{R}^2\left(z\mathbb{C}\left(\mathbf{s}_{1:2}\right)\right)\right]_{\vec{\mathbf{F}}}, \tag{20}$$

for any complex number $z \in \mathbb{C}$.

Note that

$$\mathbb{R}^{2\times2}(x+yi) \coloneqq \begin{bmatrix}x & -y\\ y & x\end{bmatrix}, \text{ and} \tag{21}$$

$$\mathbb{C}\left(\begin{bmatrix}x\\ y\end{bmatrix}\right) \coloneqq x + yi. \tag{22}$$

Denoting $\mathbf{r}_{1:10} \coloneqq \mathrm{S2L2}_{1:2}\left(\overleftrightarrow{s}_{1:2}\right)$ and $\mathbf{r}'_{1:10} \coloneqq \mathrm{S2L2}_{1:2}\left(z\overleftrightarrow{s}_{1:2}\right)$, now we can state $\mathbb{C}$-linearity of the S2L2 representation:

$$r'_{2k-1} + ir'_{2k} = z\left(r_{2k} + r_{2k+1}\right) \text{ for } i = 1,\cdots,5 \tag{23}$$

Continuity. Continuity is also straightforward regarding Equation (7).

Global Coordinate Conversion for S2L2 Representation. Before proving rotation invariance of Euclidean metric of S2L2 representations, we propose another useful formula. Suppose that $\mathbf{r} = \mathrm{S2L2}\left(\overleftrightarrow{s}\right)$ is a S2L2 representation of a Stokes vector $\overleftrightarrow{s} = [\mathbf{s}]_{\vec{\mathbf{F}}}$. Recall that rotation of a Stokes vector $\overleftrightarrow{s}$ by $\vec{R}$ is defined by [Yi et al. 2024]:

$$\vec{R}_{\mathcal{S}}\overleftrightarrow{s} \coloneqq [\mathbf{s}]_{\vec{R}\vec{\mathbf{F}}}\,. \tag{24}$$

Note that it can also indicate global coordinate (world coordinate) conversion. Then the new S2L2 representation $\mathbf{r}' = \mathrm{S2L2}\left(\vec{R}_{\mathcal{S}}\overleftrightarrow{s}\right)$ can be evaluated by:

$$r'_0 = r_0, \tag{25a}$$

$$r'_{2m+5} + ir'_{2m+6} = \sum_{m'=-2}^{2} D_{mm'}\left(\vec{R}\right)\left(r_{2m'+5} + ir_{2m'+6}\right) \text{ for } -2 \le m \le 2, \tag{25b}$$

$$r'_{11} = r_{11}. \tag{25c}$$

Proof: We need rotation property of spin-2 spherical harmonics [Boyle 2013; Yi et al. 2024]:

$${}_2Y_{lm}\left(\vec{R}\vec{\mathbf{F}}\right) = \sum_{m'=-l}^{l} D^*_{mm'}\left(\vec{R}\right){}_2Y_{lm}\left(\vec{\mathbf{F}}\right). \tag{26}$$

r_0 and r_{11} are trivial, so we only need to show $r_1 ... r_{10}$.

$$\begin{aligned} r'_{2m+5} + ir'_{2m+6} &= \sqrt{\frac{4\pi}{5}}\, {}_2Y_{2m}\left(\vec{R}\vec{\mathbf{F}}\right)^* (s_1 + is_2) \\ &= \sqrt{\frac{4\pi}{5}} \sum_{m'=-2}^{2} D_{mm'}\left(\vec{R}\right) {}_2Y_{2m'}\left(\vec{\mathbf{F}}\right)^* (s_1 + is_2) \\ &= \sum_{m'=-2}^{2} D_{mm'}\left(\vec{R}\right) (r_{2m+5} + ir_{2m+6}) \end{aligned} \tag{27}$$

□

In matrix notations, Equation (25) can be rewritten as follows:

$$\mathbf{r}' = \mathbf{R}_{\mathrm{S2L2}}\left(\vec{R}\right)\mathbf{r}, \text{ where} \tag{28}$$

$$\mathbf{R}_{\mathrm{S2L2}}\left(\vec{R}\right) := \begin{bmatrix} 1 & \mathbf{0}_{1\times 2} & \cdots & \mathbf{0}_{1\times 2} & 0 \\ \mathbf{0}_{2\times 1} & \mathbb{R}^{2\times 2}\left(D_{-2,-2}\left(\vec{R}\right)\right) & \cdots & \mathbb{R}^{2\times 2}\left(D_{-22}\left(\vec{R}\right)\right) & \mathbf{0}_{2\times 1} \\ \vdots & \vdots & \ddots & \vdots & \vdots \\ \mathbf{0}_{2\times 1} & \mathbb{R}^{2\times 2}\left(D_{2,-2}\left(\vec{R}\right)\right) & \cdots & \mathbb{R}^{2\times 2}\left(D_{22}\left(\vec{R}\right)\right) & \mathbf{0}_{2\times 1} \\ 0 & \mathbf{0}_{1\times 2} & \cdots & \mathbf{0}_{1\times 2} & 1 \end{bmatrix} \tag{29}$$

$$\in \mathbb{R}^{12\times 1}.$$

Rotation invariance of S2L2 metric. Now we provide proof for rotation invariance of metric on S2L2 representations.

Proof: Suppose that there are two Stokes vectors $\overleftrightarrow{s} = [\mathbf{s}]_{\vec{\mathbf{F}}}$ and $\overleftrightarrow{t} = [\mathbf{t}]_{\vec{\mathbf{G}}}$, not needed to have the same ray direction. Fisrt, Euclidean distance between two S2L2 vectors can be evaluated as:

$$\begin{aligned} d_{\mathrm{S2L2}}\left(\vec{R}_{\mathcal{S}}\overleftrightarrow{s}, \vec{R}_{\mathcal{S}}\overleftrightarrow{t}\right)^2 &= \left\| \mathbf{R}_{\mathrm{S2L2}}\left(\vec{R}\right) \mathrm{S2L2}\left(\vec{R}_{\mathcal{S}}\overleftrightarrow{s}\right) - \mathbf{R}_{\mathrm{S2L2}}\left(\vec{R}\right) \mathrm{S2L2}\left(\vec{R}_{\mathcal{S}}\overleftrightarrow{t}\right) \right\|_2^2 \\ &= \mathbf{R}_{\mathrm{S2L2}}\left(\vec{R}\right) \mathbf{R}_{\mathrm{S2L2}}\left(\vec{R}\right)^T \left\| \mathrm{S2L2}\left(\overleftrightarrow{s}\right) - \mathrm{S2L2}\left(\overleftrightarrow{t}\right) \right\|_2^2. \end{aligned} \tag{30}$$

We only need to show $\mathbf{R}_{\mathrm{S2L2}}\left(\vec{R}\right)\mathbf{R}_{\mathrm{S2L2}}\left(\vec{R}\right)^T = \mathbf{I}$, i.e., it is an orthogonal matrix. We observe that $\mathbf{R}_{\mathrm{S2L2}}$, defined in Equation (29), is a block-diagonal (1×1, 10×10, and 1×1) matrix, elements $\left(\mathbf{R}_{\mathrm{S2L2}}\mathbf{R}_{\mathrm{S2L2}}^T\right)_{ij}$ for either $i \neq 0, 11$ or $j \neq 0, 11$ trivially match to the identity matrix. The remain terms are cases of $1 \leq i, j \leq 10$:

$$\begin{aligned} \left(\mathbf{R}_{\mathrm{S2L2}}\mathbf{R}_{\mathrm{S2L2}}^T\right)_{ij} &= \sum_{m=-2}^{2} \mathbb{R}^{2\times 2}\left(D_{im}\left(\vec{R}\right)\right) \mathbb{R}^{2\times 2}\left(D_{mj}\left(\vec{R}\right)\right)^T \\ &= \sum_{m=-2}^{2} \mathbb{R}^{2\times 2}\left(D_{im}\left(\vec{R}\right) D^*_{mj}\left(\vec{R}\right)\right). \end{aligned} \tag{31}$$

Here, we can utilize the following identity for Wigner D-matrices:

$$\sum_{m=-2}^{2} D_{im}\left(\vec{R}\right) D^*_{mj}\left(\vec{R}\right) = \delta_{ij}. \tag{32}$$

Then we get $\left(\mathbf{R}_{\mathrm{S2L2}}\mathbf{R}_{\mathrm{S2L2}}^T\right)_{ij} = \delta_{ij}$, i.e., $\mathbf{R}_{\mathrm{S2L2}}$ is an orthogonal matrix. □

D NUMERICAL VALIDATION FOR PROPERTIES

D.1 Continuity validation

While continuity of the S2L2 representation and rotation invariance of d_{S2L2} follow directly from their definitions, we additionally validate these properties through numerical experiments to confirm the correctness of our theoretical derivations and implementation. We first construct an experimental dataset consisting of uniformly distributed spin-2 Stokes vectors, denoted by S. Specifically, we select $N = 1,000$ ray directions $\hat{\omega}_1, \ldots, \hat{\omega}_N \in \hat{\mathbb{S}}^2$ using the spherical Fibonacci point set [Hannay and Nye 2004; Svergun 1994]. For each direction $\hat{\omega}_i$, we define four Stokes component vectors aligned with directions $[1,0]^T$, $[0,1]^T$, $[-1,0]^T$, and $[0,-1]^T$ in the $\theta\phi$ frame field, yielding a total of $4N$ spin-2 Stokes vectors.

For each vector $\overleftrightarrow{s} \in S$, as illustrated in Figure 1(a), we introduce small perturbations by rotating it around each axis $\hat{\omega}_1, \ldots, \hat{\omega}_N$ by 0.1, rad, i.e., $\vec{R}_i = \vec{R}_{\hat{\omega}_i}(0.1, \mathrm{rad})$. To quantitatively assess the sensitivity of different numerical representations to these perturbations, we compute the maximum perturbation-induced distance, defined as $\max_{\vec{R}_i} d\left(\overleftrightarrow{s}, \vec{R}_i\overleftrightarrow{s}\right)$ for each vector $\overleftrightarrow{s}$, and summarize these results in the histogram presented in Figure 1(b).

For comparison, we evaluate two conventional frame-dependent representations using the standard Euclidean distance in Stokes parameter space:

$$d_{\vec{\mathbf{F}}}\left(\overleftrightarrow{s}, \overleftrightarrow{t}\right) = \left\| \left[\overleftrightarrow{s}\right]^{\vec{\mathbf{F}}} - \left[\overleftrightarrow{t}\right]^{\vec{\mathbf{F}}} \right\|_2.$$

Specifically, the first plot employs the commonly used $\theta\phi$ frame field, while the second plot utilizes the frame field proposed by Duff et al. [2017], frequently adopted in recent polarized graphics research [Jakob et al. 2022; Kim et al. 2023]. The third plot illustrates results obtained using our proposed S2L2 distance metric from Equation (20).

The histograms clearly highlight the numerical instability and non-uniformity inherent to conventional frame-dependent methods (first and second plots in Figure 1(b)). Notably, several vectors exhibit a maximum distance of 2, indicating that perturbations caused frame-dependent representations to flip Stokes vectors to opposite orientations, a phenomenon occurring near frame-field singularities. In contrast, our S2L2 representation consistently shows uniform perturbation-induced distances around 0.2, a magnitude ten times smaller, with negligible numerical error ($\pm 10^{-14}$).

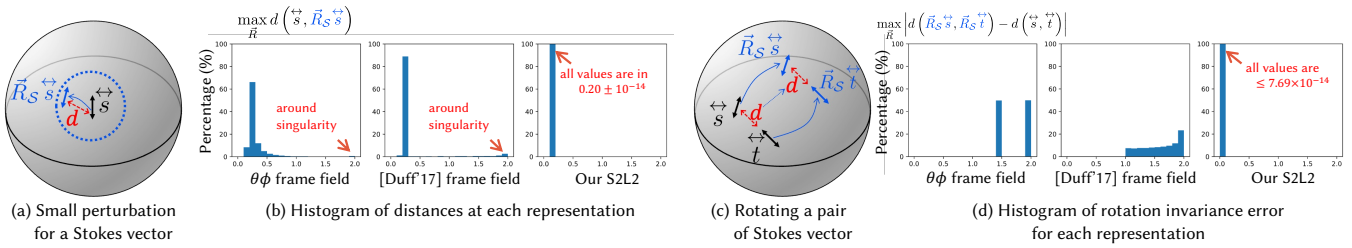

(a) Small perturbation for a Stokes vector

(b) Histogram of distances at each representation

(c) Rotating a pair of Stokes vector

(d) Histogram of rotation invariance error for each representation

Fig. 1. We introduce the *S2L2 representation*, a novel, frame-free representation of Stokes vectors. Here, we numerically validate its performance against the conventional Stokes-component representation defined under the $\theta\phi$ frame field and the frame field proposed by Duff et al. [2017]. Our method exhibits improved numerical stability under small perturbations of Stokes vectors (a) and (b), as well as rotation-invariant distance measurement (c) and (d). Note that since our evaluation uses unit-norm Stokes vectors, the value of 2.0 on the x-axis represents the theoretical maximum possible value.

D.2 Rotation invariance validation

We further numerically examine rotation invariance properties. As depicted in Figure 1(c), for each pair of vectors $\overleftrightarrow{s}, \overleftrightarrow{t} \in S$, we measure the variation of their computed distance under rotations. Specifically, we compute:

$$\max_{\vec{R}} \left| d\left(\vec{R}_{\mathcal{S}}\overleftrightarrow{s}, \vec{R}_{\mathcal{S}}\overleftrightarrow{t}\right) - d\left(\overleftrightarrow{s}, \overleftrightarrow{t}\right)\right|,$$

where the maximum is taken over rotations $\vec{R} = \vec{R}_{\hat{\omega}_i}(\theta_j)$ with angles θ_j evenly spaced over the interval $[0, 2\pi)$.

Figure 1(d) provides a histogram summarizing these maximum rotation-induced distance variations for each Stokes vector. The first two plots, corresponding to conventional frame-dependent methods, exhibit significant variability, clearly demonstrating their lack of rotation invariance. Conversely, the third plot, corresponding to our S2L2 representation, confirms its near-perfect rotation invariance, showing only negligible numerical discrepancies on the order of 7.69×10^{-14}.

E STANDARDIZING VISUALIZATION OF STOKES VECTOR FIELDS

In Section 5, we visualize equirectangular images of a Stokes parameters with respect to the $\phi\theta$-frame field $\vec{\mathbf{F}}_{\theta\phi}$. In this case, the continuity the Stokes vector field implied continuity of equirectangular images of each Stokes component, and the only difference between continuities of scalar fields and Stokes vector fields appears in the boundary of equirectangular images. This property arises because the singularities of the $\theta\phi$-frame field is located along the boundary of the equirectangular image representation, providing a natural visualization of Stokes vector fields.

However, there are various choices to represent spherical images into planar images such as perspective images of certain ranges of the entire sphere, cube maps, mirror ball representations, which is equivalent to capturing a chrome ball object that reflects environment lighting, octahedron maps, and orthogonal projections of two hemispheres as shown in Figure 2. With various options available for spatial representation a spherical image on a plane, and numerous choices of frame fields that influence the values of Stokes components, the number of possible visualization methods for a Stokes vector field into planar images becomes exceedingly large. To reduce this variety of conventions, we propose standardized choices frame fields for each spatial representation.

Similar to the usage of $\theta\phi$-frame field for equirectangular maps, our main focus to standardizing choices of frame fields would be putting the singularities of frame fields only at the boundary of warped planar images of a Stokes vector field. Positions at the sphere of such boundaries are illustated in the top row of Figure 2. For perspective images, we use the Mitsuba-perspective frame field[1] $\vec{\mathbf{F}}_{\text{pers}}(\hat{\omega})$ shown in Figure 4(b), characterized by the up vectors of the perspective cameras. Note that there are several choices of such camera-based frame field conventions. We follow the convention of Mitsuba 3 renderer [Jakob et al. 2022], which is defined as follows.

$$\begin{aligned}\vec{\mathbf{F}}_{\text{pers}}(\hat{\omega}; \hat{u}) &= \left[\hat{x}_{\text{pers}}(\hat{\omega}) \quad \hat{y}_{\text{pers}}(\hat{\omega}) \quad \hat{\omega}\right], \\ \hat{x}_{\text{pers}} &= \text{normalize}(\hat{u} \times \hat{\omega}), \\ \hat{y}_{\text{pers}} &= \hat{\omega} \times \hat{x}_{\text{pers}}.\end{aligned} \tag{33}$$

When $\hat{u} = \hat{z}_g$, this frame field can be visualized as Figure 4(b).

For the cube map representation (Figure 2(b)), we define the *cubemap frame field*, which consists of six segments of Mitsuba-perspective frame fields:

$$\vec{\mathbf{F}}_{\text{cube}}(\hat{\omega}) = \begin{cases} \vec{\mathbf{F}}_{\text{pers}}(\hat{\omega}; \hat{u} = -\hat{y}_g) & \text{if } \hat{\omega} \text{ belongs to the top face} \\ \vec{\mathbf{F}}_{\text{pers}}(\hat{\omega}; \hat{u} = \hat{y}_g) & \text{if } \hat{\omega} \text{ belongs to the bottom face} \\ \vec{\mathbf{F}}_{\text{pers}}(\hat{\omega}; \hat{u} = \hat{z}_g) & \text{otherwise} \end{cases}. \tag{34}$$

This is also illustrated in Figure 2(c). Visualizing a Stokes vector field as cube map images with respect to $\vec{\mathbf{F}}_{\text{cube}}$ is the only exception, among the standard conventions we propose, that includes frame field singularities within the interior of cube map images. For further discussion, refer to Section E.1.

For mirror ball and octahedron maps (Figure 2(c and d)), we use the *geodesic frame field* $\vec{\mathbf{F}}_{\text{geo}}(\hat{\omega})$, which is obtained as the parallel transport of $\vec{\mathbf{F}}_g$, regarded by a local frame at $\hat{z}_g$, to $\hat{\omega}$ along a geodesic curve. It can be also simply written as follows.

$$\vec{\mathbf{F}}_{\text{geo}}(\theta, \phi) = \vec{R}_{\hat{z}_g \hat{y}_g \hat{z}_g}(\phi, \theta, -\phi)\, \vec{\mathbf{F}}_g. \tag{35}$$

As also seen in Figure 4(d), it has only a single degenerate singular point with winding number 2.

[1]Note that this frame field was referred to simply as the *perspective frame field* in prior work [Yi et al. 2024]. However, other work [Kim et al. 2023] adopts a different convention: a rotated version of Duff et al. [2017]'s frame field aligned with the camera coordinate system. To clarify that this is not a unique or canonical choice, we refer to the one used in our experiment as the *Mitsuba-perspective* frame field.

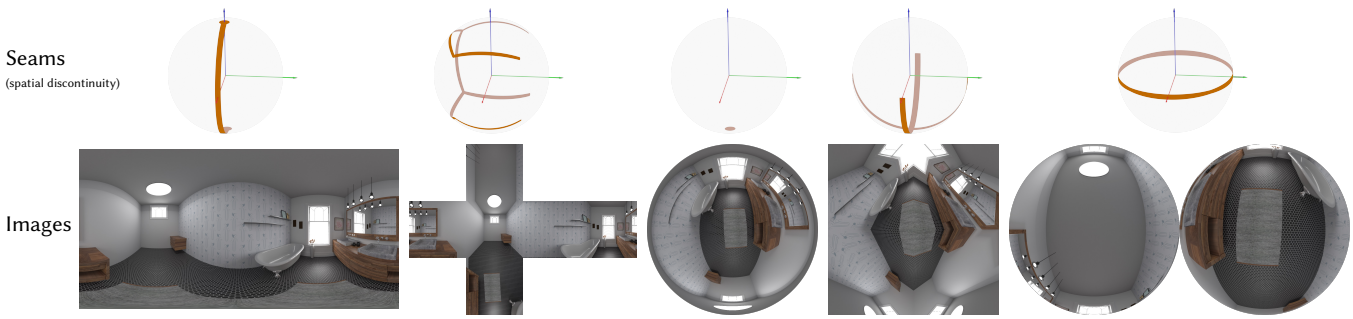

Fig. 2. There are several kinds of mappings from the entire sphere to a plane for visualizing spherical functions. Yellow points and curves on the top row indicate spatial discontinuities of such mappings. The bottom row indicates environment map image in each convention.

Finally, for orthographic projections of hemispheres (Figure 2(e)), we use Duff et al. [Duff et al. 2017]'s frame field $\vec{\mathbf{F}}_{[\text{Duff}]}(\hat{\omega})$. While Duff et al. mainly focuses on numerically stable computation, the frame field itself can also be written as a simpler formula:

$$\vec{\mathbf{F}}_{[\text{Duff}]}(\hat{\omega}) = \begin{cases} \vec{\mathbf{F}}_{\text{geo}}(\hat{\omega}) & \text{if } \hat{z}_g \cdot \hat{\omega} \geq 0 \\ \vec{R}_{\hat{x}_g}(\pi)\,\vec{\mathbf{F}}_{\text{geo}}\left(\vec{R}_{\hat{x}_g}(\pi)\,\hat{\omega}\right) & \text{if } \hat{z}_g \cdot \hat{\omega} < 0 \end{cases}. \tag{36}$$

As seen in Figure 4(e), its singularity is the equator of the sphere, which is identical to the spatial discontinuity of the hemisphere projections. Note that Duff et al.'s frame field is also used in Mitsuba 3 renderer to numerically represent Stokes vectors of each direction of rays.

Using the proposed choices of frame fields, we finally get Stokes vector field visualizations as shown in Figure 2.

E.1 Discussion on Alternative Choices

$\theta\phi$- vs. $\phi\theta$-frame fields for the equirectangular map. For equirectangular representation, we propose another choice of frame field, named $\phi\theta$-frame field, which can be obtained by rotating each local frame of the $\theta\phi$-frame field around its local z axis by 90°.

$$\begin{aligned} \vec{\mathbf{F}}_{\phi\theta}(\hat{\omega}) &= \begin{bmatrix} \hat{x}_{\phi\theta}(\hat{\omega}) & \hat{y}_{\theta\phi}(\hat{\omega}) & \hat{\omega} \end{bmatrix} = \vec{R}_{\hat{\omega}}\left(\frac{\pi}{2}\right)\vec{\mathbf{F}}_{\theta\phi}(\hat{\omega}) \\ \hat{x}_{\phi\theta}(\hat{\omega}) &= \text{normalize}\left(\frac{\partial \hat{\omega}_{\text{sph}}(\theta,\phi)}{\partial \phi}\right) = \vec{\mathbf{F}}_g \begin{bmatrix} -\sin\phi & \cos\phi & 0 \end{bmatrix}^T, \\ \hat{y}_{\phi\theta}(\hat{\omega}) &= -\frac{\partial \hat{\omega}_{\text{sph}}(\theta,\phi)}{\partial \theta} = \vec{\mathbf{F}}_g \begin{bmatrix} -\cos\theta\cos\phi & -\cos\theta\sin\phi & \sin\theta \end{bmatrix}^T. \end{aligned} \tag{37}$$

Both $\theta\phi$- and $\phi\theta$-frame fields do not contain interior singularities on equirectangular maps. The $\theta\phi$-frame field offers mathematical conveniences. In differential geometry, it is common to choose a local frame at a point on a manifold as the derivatives of a parametrization. From this perspective, it is natural to define the first and second axes to be parallel to $\frac{\partial \hat{\omega}_{\text{sph}}}{\partial \theta}$ and $\frac{\partial \hat{\omega}_{\text{sph}}}{\partial \phi}$, respectively, as spherical coordinates are typically enumerated in the θ, ϕ order. Additionally, a convenient formula relates this frame field to the ZYZ Euler angles, as shown in Equation (1a) in the appendix. Existing literature [Goldberg et al. 1967; Ng and Liu 1999] also adopts the $\theta\phi$-frame field for formulating spin-2 spherical harmonics.

However, viewers of a planar visualization of Stokes vector fields may naturally assume that the "horizontal" and "vertical" directions of polarization align with the horizontal and vertical directions of the image plane, respectively. In this context, the $\theta\phi$-frame field can feel counterintuitive, as the $\hat{x}_{\theta\phi}(\theta)$ and $\hat{y}_{\theta\phi}(\phi)$ axes are typically aligned with the vertical and horizontal directions of the equirectangular image plane, respectively. From this perspective, the $\phi\theta$-frame field offers a more intuitive alignment, with the $\hat{x}_{\phi\theta}$ and $\hat{y}_{\phi\theta}$ axes perfectly matching those of the image plane.

Additionally, note that the $\phi\theta$ and the Mitsuba-perspective frame fields are identical when $\hat{u} = \hat{z}_g$. However, we use both terms with their respective names to emphasize their distinct usages.

Perspective images. While frame fields on the sphere must contain singularities somewhere in the directional domain, perspective images only require that no singularities exist within the field of view. Previous works such as Jakob et al. [2022]; Yi et al. [2024] used the *Mitsuba-perspective frame field*, which aligns the global $\hat{z}_g$ axis of the $\theta\phi$-frame field with the camera's up vector. In contrast, Kim et al. [2023] employed a rotated version of the Duff et al. [2017] frame field, aligning its global axes $\hat{x}_g$, $\hat{y}_g$, and $\hat{z}_g$ with the camera's right, up, and back directions, respectively.

Both conventions are acceptable. In this paper, for consistency and ease of implementation, we use the rotated Duff et al. [2017]'s frame field in the results shown in Section 6, and the Mitsuba-perspective frame field for visualizations in all other figures.

Interior singularities in the cube map. As shown in Figure 4(c), the cubemap frame field $\vec{\mathbf{F}}_{\text{cube}}(\hat{\omega})$ exhibits singularities at the two spherical rectangles forming the boundaries of the top and bottom faces. However, some sides of these rectangles do not correspond to spatial discontinuities in the cube map representation (Figure 2(b)). This results in discontinuities in the Stokes components, as illustrated by the magenta dotted lines in Figure 3(c).

This raises the question of when to use cube map warping. The primary advantage of the cube map is its compatibility with perspective images. For example, a cube map image can be easily generated

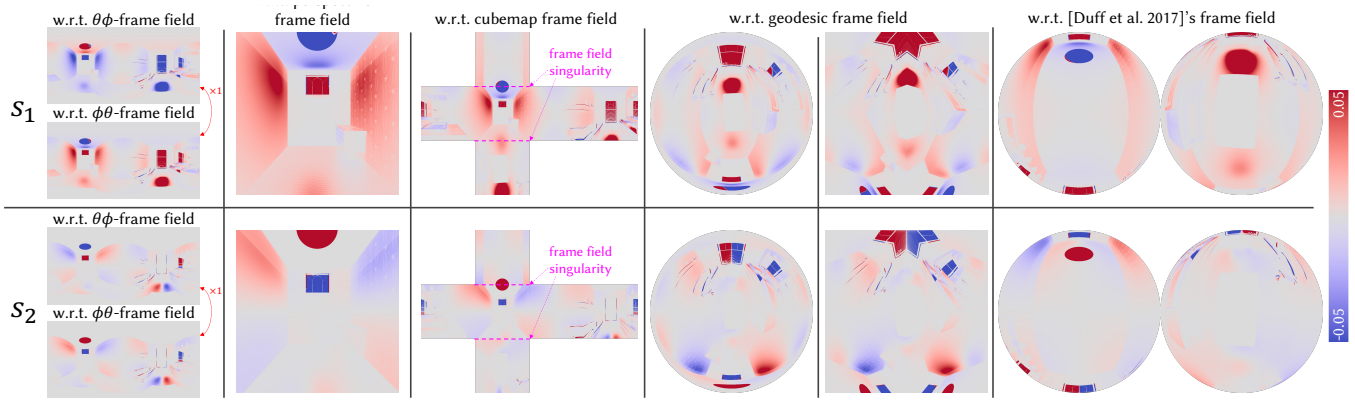

Fig. 3. We propose standard choices of frame fields to visualize Stokes vector fields for each spherical mapping in Figure 2. Excepting cube map warping with the cubemap frame field in (c), all other visualizations use frame fields that only have singularities at the boundary of each of warped planar images. For a discussion on the two options for the equirectangular map and the interior frame field singularities for the cube map, see Section E.1.

by concatenating six perspective images captured from six camera poses, whether for rendering using a system that only supports perspective cameras or for capturing environment lighting with a perspective camera device. Thus, we recommend using the cubemap frame field for the cube map spatial warping, prioritizing compatibility with perspective visualization over the elimination of interior frame field singularities.

F APPLICATION: POLARIZED RADIANCE FIELD

Figure 5 and Figure 6 show the results of singularity with respect to the camera translation and the camera rotation.

REFERENCES

Michael Boyle. 2013. Angular velocity of gravitational radiation from precessing binaries and the corotating frame. *Physical Review D* 87, 10 (2013), 104006.

Tom Duff, James Burgess, Per Christensen, Christophe Hery, Andrew Kensler, Max Liani, and Ryusuke Villemin. 2017. Building an orthonormal basis, revisited. *JCGT* 6, 1 (2017).

Joshua N Goldberg, Alan J MacFarlane, Ezra T Newman, Fritz Rohrlich, and EC George Sudarshan. 1967. Spin-s Spherical Harmonics and ð. *J. Math. Phys.* 8, 11 (1967), 2155–2161.

JH Hannay and JF Nye. 2004. Fibonacci numerical integration on a sphere. *Journal of Physics A: Mathematical and General* 37, 48 (2004), 11591.

Wenzel Jakob, Sébastien Speierer, Nicolas Roussel, Merlin Nimier-David, Delio Vicini, Tizian Zeltner, Baptiste Nicolet, Miguel Crespo, Vincent Leroy, and Ziyi Zhang. 2022. *Mitsuba 3 renderer.* https://mitsuba-renderer.org.

Youngchan Kim, Wonjoon Jin, Sunghyun Cho, and Seung-Hwan Baek. 2023. Neural Spectro-Polarimetric Fields. In *SIGGRAPH Asia 2023 Conference Papers.*

Michal Mojzík, Tomáš Skřivan, Alexander Wilkie, and Jaroslav Křivánek. 2016. Bi-directional polarised light transport. In *Proceedings of the Eurographics Symposium on Rendering: Experimental Ideas & Implementations.* 97–108.

Kin-Wang Ng and Guo-Chin Liu. 1999. Correlation functions of CMB anisotropy and polarization. *International Journal of Modern Physics D* 8, 01 (1999), 61–83.

DI Svergun. 1994. Solution scattering from biopolymers: advanced contrast-variation data analysis. *Acta Crystallographica Section A: Foundations of Crystallography* 50, 3 (1994), 391–402.

Shinyoung Yi, Donggun Kim, Jiwoong Na, Xin Tong, and Min H Kim. 2024. Spin-Weighted Spherical Harmonics for Polarized Light Transport. *ACM Transactions on Graphics (TOG)* 43, 4 (2024), 1–24.

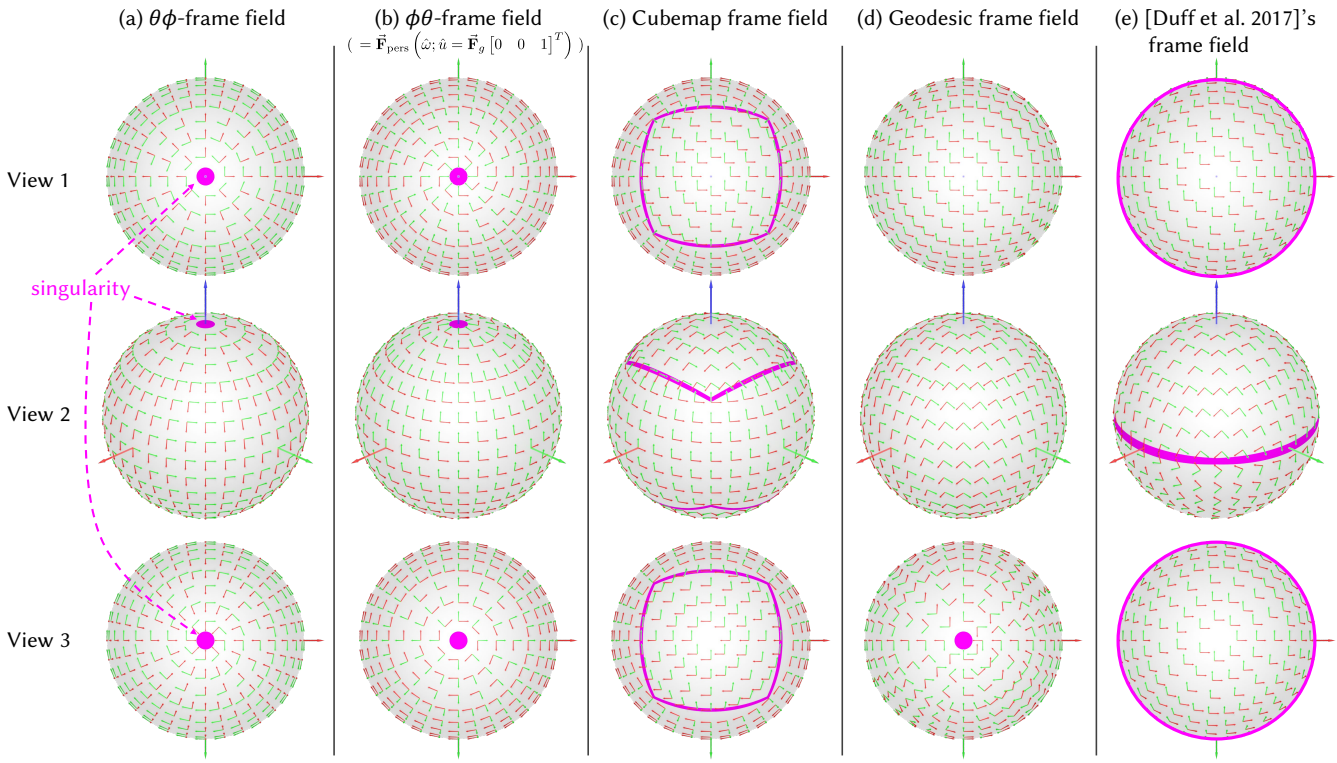

Name	Definition	Dependency	Singularities	
$\theta\phi$-frame field $\vec{\mathbf{F}}_{\theta\phi}\ (\hat{\omega})$	Eq. (1a)	Global z-axis $\hat{z}_g$	$\hat{\omega} = \pm\hat{z}_g$	Fig. 4(a)
$\phi\theta$-frame field $\vec{\mathbf{F}}_{\phi\theta}\ (\hat{\omega})$	Eq. (37)	Global z-axis $\hat{z}_g$	$\hat{\omega} = \pm\hat{z}_g$	Fig. 4(b)
Perspective frame field $\vec{\mathbf{F}}_{\text{pers}}\ (\hat{\omega}; \hat{u})$	Eq. (33)	Camera up vector $\hat{u}$	$\hat{\omega} = \pm\hat{u}$	Fig. 4(b)
Cubemap frame field $\vec{\mathbf{F}}_{\text{cube}}\ (\hat{\omega})$	Eq. (34)	Global frame $\vec{\mathbf{F}}_g$	Two spherical rectangles	Fig. 4(c)
Geodesic frame field $\vec{\mathbf{F}}_{\text{geo}}\ (\hat{\omega})$	Eq. (35)	Global frame $\vec{\mathbf{F}}_g$	$\hat{\omega} = -\hat{z}_g$	Fig. 4(d)
Duff et al. [2017]'s $\vec{\mathbf{F}}_{[\text{Duff}]}\ (\hat{\omega})$	Eq. (36)	Global frame $\vec{\mathbf{F}}_g$	The equator ($\hat{\omega} \cdot \hat{z}_g = 0$)	Fig. 4(e)

Fig. 4. Several conventions to choose a frame field for visualization of Stokes vector fields. Each frame field may have singularities at different positions. Figure 4 in our supplementary material contains an extended version of this figure. This is also an extended version of Figure 2 in our main paper. Several conventions to choose a frame field for visualization of Stokes vector fields. Each frame field may have singularities at different positions.

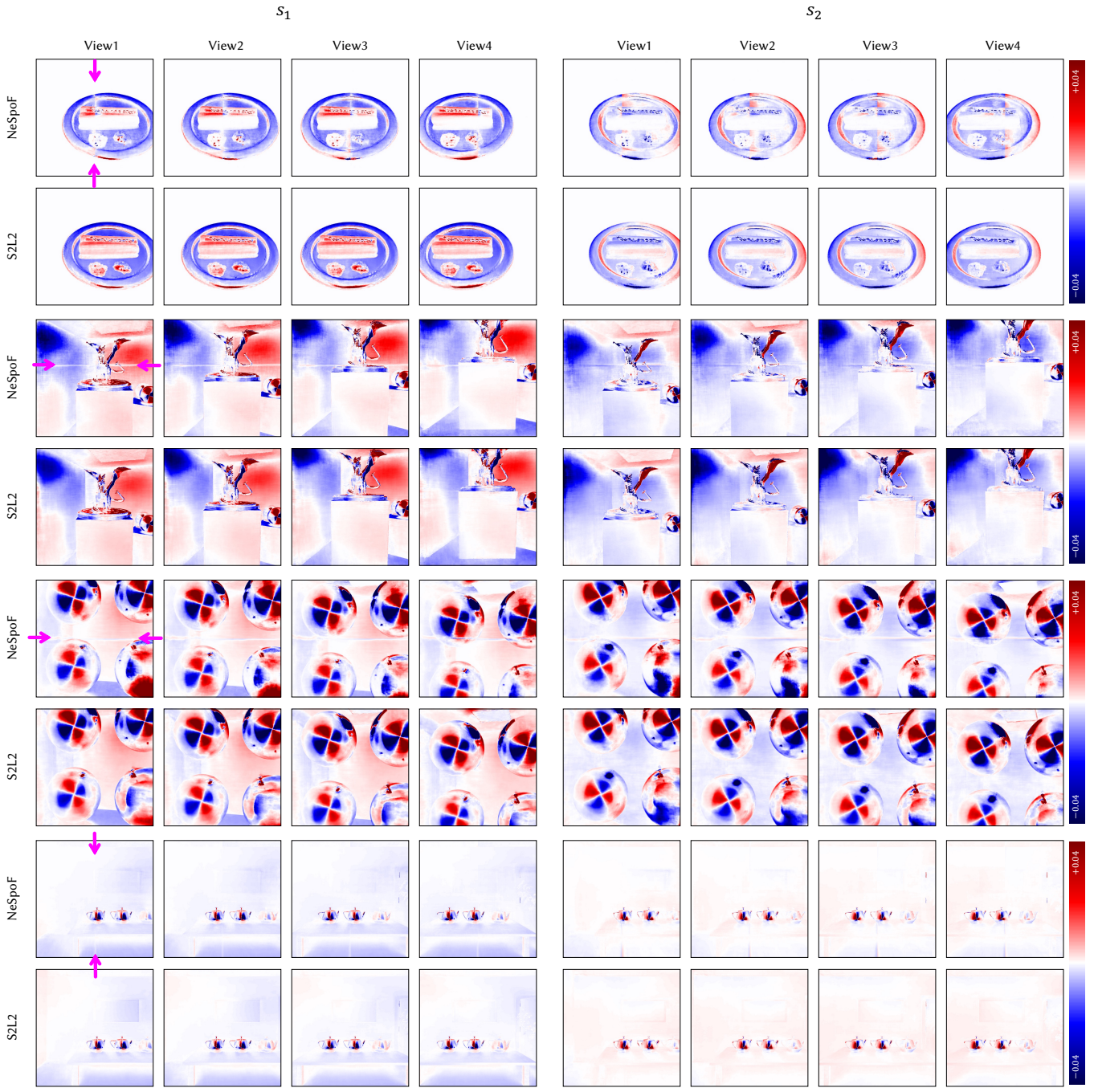

Fig. 5. Rendered images by translating the camera. The magenta arrows indicate the singularity.

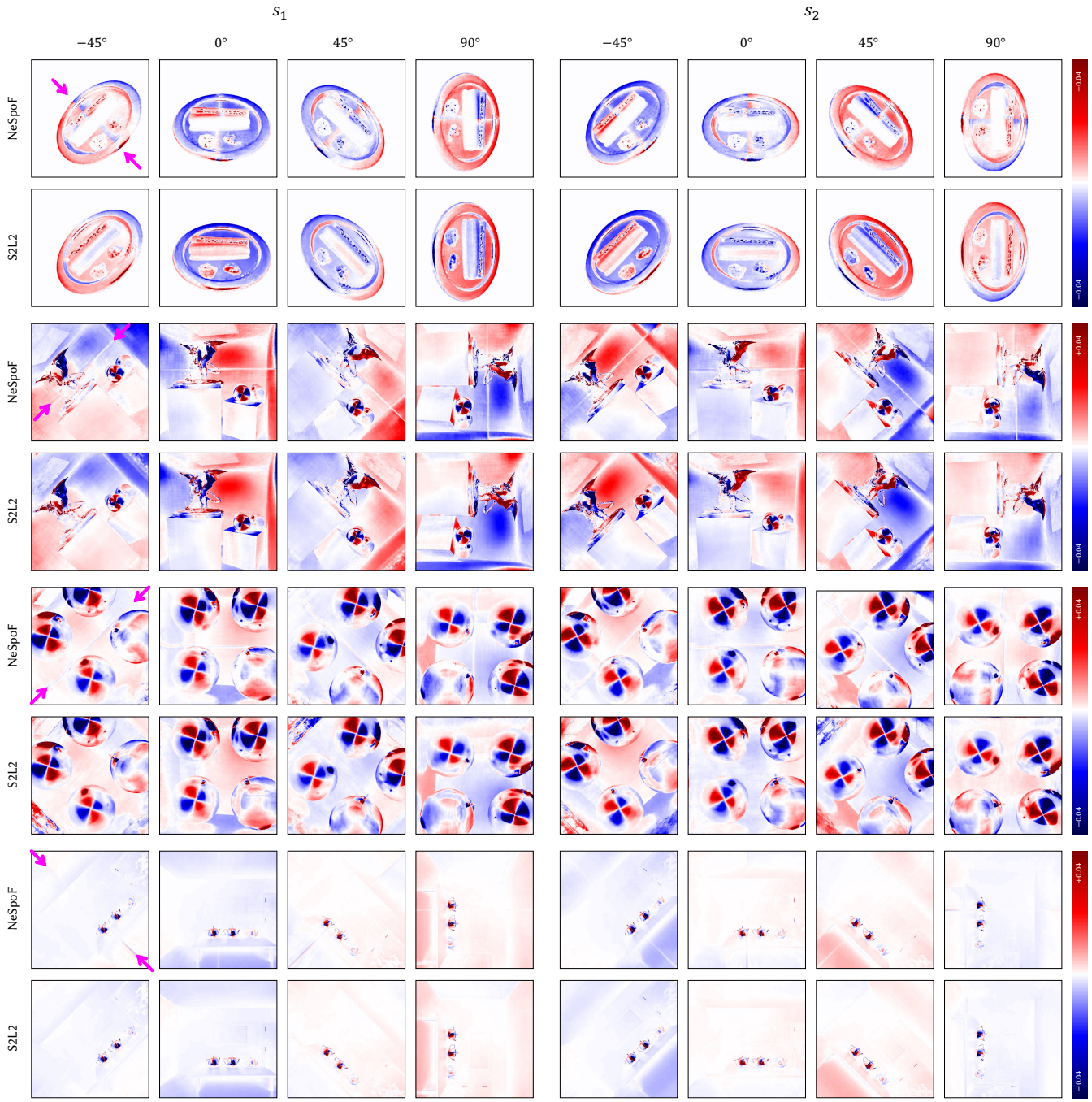

Fig. 6. Rendered images by rotating the camera. The magenta arrows indicate the singularity.